Study of optical constants in PbSrSe thin films for mid-infrared laser application

2002 J. Phys.: Condens. Matter 14 2067

(http://iopscience.iop.org/0953-8984/14/8/332)

INSTITUTE OF PHYSICS PUBLISHING JOURNAL OF PHYSICS: CONDENSED MATTER

J. Phys.: Condens. Matter **14** (2002) 2067–2078 PII: S0953-8984(02)28769-X

Study of optical constants in PbSrSe thin films for mid-infrared laser application

H F Yang, W Z Shen[1] and Q J Pang

Laboratory of Condensed Matter Spectroscopy and Opto-Electronic Physics,
Department of Physics, Shanghai Jiao Tong University, 1954 Hua Shan Road, Shanghai 200030,
People's Republic of China

Received 12 September 2001, in final form 31 December 2001
Published 15 February 2002
Online at stacks.iop.org/JPhysCM/14/2067

Abstract

Spectroscopy measurements of optical constants of molecular-beam-epitaxy-grown PbSrSe thin films have been carried out for mid-infrared laser application. A new and simple empirical model for the refractive index and extinction coefficient of $Pb_{1-x}Sr_xSe$ thin films, in relation to the band-gap energy, is presented. The model of the optical constants is based on the Lorentz calculation of the imaginary part of the dielectric function. In contrast to other models, our model not only can explain well all of our experimental results with Sr compositions as high as 0.276 and at different temperatures from 10 to 300 K, but also is in good agreement with the reported results for PbSrSe thin films in the literature. Furthermore, we obtain, for the first time, the SrSe thermal expansion coefficient: $(7.3 \pm 0.3) \times 10^{-6}$ K^{-1}, based on the model and experimental data. The results clearly show promise of being applicable to PbSrSe thin films as well as their microstructures.

1. Introduction

IV–VI semiconductors have several unique properties that make them attractive for mid-infrared laser fabrication. In contrast to III–V and II–VI semiconductors, IV–VI lead salts have multi-valley band structure with the band extreme at the L point of the Brillouin zone. The absence of a heavy-hole band can reduce the non-radiative Auger recombination rate drastically, to values one or two orders of magnitude lower than those for narrow-gap III–V and II–VI materials [1, 2], and favourably influences the high-temperature threshold current. The lower density of states and stronger interband matrix elements allow the appearance of stimulated emission at relatively low generation rates. In the past few years, efforts to improve IV–VI semiconductor laser performance have been hindered by the limited availability of IV–VI semiconductor materials and by the limited knowledge of material parameters as well. The recent development of growth technologies, such as liquid-phase epitaxy (LPE)

[1] Author to whom any correspondence should be addressed.

and molecular-beam-epitaxy (MBE), for IV–VI semiconductors on low-cost BaF_2 or silicon substrates [3–5] offers new opportunities for producing novel IV–VI semiconductor materials and opto-electronic devices based on them. In particular, strong continuous-wave room temperature (RT) stimulated emission luminescence has been observed very recently [1, 2] between 3 and 4 μm from PbSe/PbSrSe multiple-quantum-well (MQW) laser structures, well above the limit of 2.3 μm for type II quantum cascade laser structures produced using narrow-gap III–V antimonide semiconductor materials. Following on from this, ternary alloy–semiconductor $Pb_{1-x}Sr_xSe$ thin films with sodium chloride structure have been paid much attention. They exhibit a direct energy gap and the energy gap increases rapidly with increasing Sr content in the PbSe matrix, which is of great interest for opto-electronic applications.

Knowledge of the refractive index is important in the design of heterostructure lasers [2, 6, 7]. For example, the refractive index for the operation of an injection laser plays a key role in the confinement of the emitted radiation to the intermediate vicinity of an active region [7]. It is also important to study the rate of change of the refractive index with temperature, dn/dT, from the temperature stability point of view for opto-electronic devices. To design the optimal device structure, it is essential to know exactly the refractive index of PbSrSe thin films. Some groups have investigated the refractive index of PbSrSe [2, 8–10]. However, to the best of our knowledge, there has been no systematic experimental and theoretical investigation of the temperature and Sr-composition-dependence of the refractive index in PbSrSe thin films. In this paper, we have carried out a detailed temperature-dependent (10–300 K) and Sr-composition-dependent (0–0.276) spectroscopy study of the optical constants for PbSrSe thin films. We present a new model that can explain well not only all of our experimental results, but also some results in the literature for PbSrSe thin films. On the other hand, the thermal expansion coefficient of SrSe is still not available in the literature [3]. From our model here, we can also get the thermal expansion coefficient of SrSe: $(7.3 \pm 0.3) \times 10^{-6}$ K^{-1}; this is achieved here for the first time.

2. Experiments

The $Pb_{1-x}Sr_xSe$ thin-film samples were grown on $BaF_2(111)$ substrates by MBE with the Sr content x equal to 0.066, 0.171, and 0.276. The thicknesses of the thin films are around 1 μm, and the Sr composition is confirmed by high-resolution x-ray diffraction (HRXRD) measurements. The infrared absorption measurements were performed on a Nicolet Nexus 870 Fourier transform infrared (FTIR) spectrometer with a DTGS detector and a variable-temperature (10–300 K) sample chamber equipped with a silicon diode sensor. The closed-cycle refrigerator system consists of a Lakeshore 321 auto-tuning temperature controller and a CTI-Cryogenics 8200 compressor. The exact thickness of the $Pb_{1-x}Sr_xSe$ epitaxial layers at RT was obtained from variable-angle spectroscopic ellipsometry (WVASE32) measurements. The experimental refractive indices at RT (300 K) for the $Pb_{1-x}Sr_xSe$ thin films were calculated via $n = (2d\,\Delta\nu)^{-1}$ where $\Delta\nu$ is the spacing of the Fabry–Pérot interference fringes found from FTIR absorption spectra, and d is the thickness of the thin films. Table 1 gives the exact thicknesses and experimental refractive indices for the three PbSrSe thin films at RT for a couple of photon energies. A comparison of the refractive indices between experiment and calculation has also been given in table 1. Then we adjust only two parameters (E_0 and $\varepsilon_1(\infty)$; see below), which are related to the band gap for every sample, in our Lorentz model to make the theoretical refractive indices at RT agree with the experimental results. In this way, we can use the set of parameters for PbSrSe thin films, which can help us to obtain the theoretical refractive index of every sample at different temperatures. Finally, we change only the thickness of the $Pb_{1-x}Sr_xSe$ thin films at different temperatures to make the experimental refractive index

Table 1. The values of the thickness and refractive index obtained from experiment and calculation for $Pb_{1-x}Sr_xSe$ thin films at 300 K.

Sample composition x	Photon energy (eV)	Calculation n	Experiment n	Experiment d (μm)
0.276	1.045	5.691	5.668	1.0921
	0.857	4.301	4.271	
	0.407	3.697	3.689	
0.171	0.659	4.719	4.606	0.8296
	0.572	4.316	4.322	
	0.486	4.095	4.093	
0.066	0.361	4.796	4.795	0.8064
	0.292	4.513	4.518	

results obtained via $n = (2d\,\Delta\nu)^{-1}$ consistent with the theoretical values. By means of these processes we can get the refractive indices and the film thicknesses at different temperatures in relation to the band gap for every sample with two fitting parameters. As a result, we can also get the SrSe thermal expansion coefficient from the change of the PbSrSe thin film thickness with temperature by means of a linear interpolation scheme, with the PbSe thermal expansion coefficient of 19.4×10^{-6} K^{-1} [1] and that of SrSe. The consistency of all the observed experimental results demonstrates strongly the reliability of both our model and our results.

It is obvious that the band gap E_g is a key parameter in determining the refractive indices. Figure 1 shows the temperature-dependent FTIR absorption results for the three samples. In addition to the Fabry–Pérot interference fringes at low energy, the absorption edges are clearly shown in the spectra. The absorption edge energies can be obtained, as is widely done in the literature [5, 10], from the intersection of the square of the absorption slope with the lowest measured absorption between the interface fringes. On the basis of the detailed temperature- and Sr-composition-dependent absorption measurements, we find that the band gap $E_g(x, T)$ for $Pb_{1-x}Sr_xSe$ thin films can be expressed as follows [11]:

$$E_g(x, T) = 0.150 + 3.608x - 1.314x^2 + (0.430 - 3.093x + 6.495x^2) \times 10^{-3}T \text{ (eV)} \quad (\text{for } 0 \leqslant x \leqslant 0.276,\ 0 < T \leqslant 350 \text{ K}). \tag{1}$$

Equation (1) was derived on the basis of the fact that the band gaps in many ternary alloys can be approximated in the form of a quadratic function of the composition x, and the band gaps are found to be linear with temperature in all three PbSrSe thin films. Equation (1) has been shown to match well with both our experimental results and data (including those for PbSe [2, 12]) reported by different groups for different growth conditions (see [2, 4, 12, 13]).

3. Model

Other groups have proposed some models to fit the refractive index for PbSrSe [8], AlGaAs [14], HgCdTe [15], and amorphous materials [16]. However, when compared with our experimental refractive index results for $Pb_{1-x}Sr_xSe$ at RT, the theoretical refractive index results obtained using these models are either larger or much smaller than the experimental data (and the change with photon energy is also quite different). Figure 2 shows the data for $Pb_{0.724}Sr_{0.276}Se$ from several models and our experimental data (filled squares). The dashed curve shows the results from the model using DiDomenico–Wemple parameters [8] and a semi-empirical formula [14]; the dotted curve below is from the Tauc–Lorentz model [16]. The solid curve shows our theoretical results, which are obviously in good agreement with our experimental data.

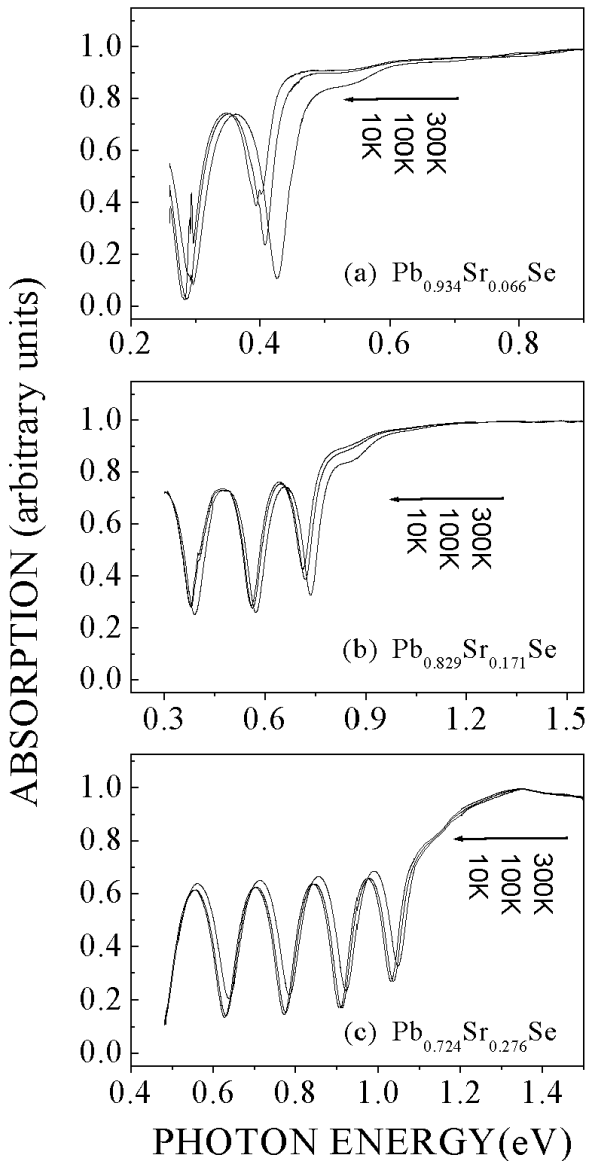

Figure 1. Temperature-dependent FTIR absorption spectra of PbSrSe thin films with different Sr compositions. (a) $Pb_{0.934}Sr_{0.066}Se$, (b) $Pb_{0.829}Sr_{0.171}Se$, (c) $Pb_{0.724}Sr_{0.276}Se$. A clear absorption edge is observed followed by below-band-gap Fabry–Pérot interference fringes for each spectrum.

In detail, our parametrization is based on a Lorentz calculation of the imaginary part of the dielectric function $\varepsilon_2(E)$ of a collection of non-interacting atoms. If only a single transition is considered, $\varepsilon_2(E)$ is given by

$$\varepsilon_2(E) = \frac{AE_0CE}{(E^2 - E_0^2)^2 + C^2E^2} \qquad E > E_g \tag{2a}$$

and

$$\varepsilon_2(E) = 0 \qquad E \leqslant E_g \tag{2b}$$

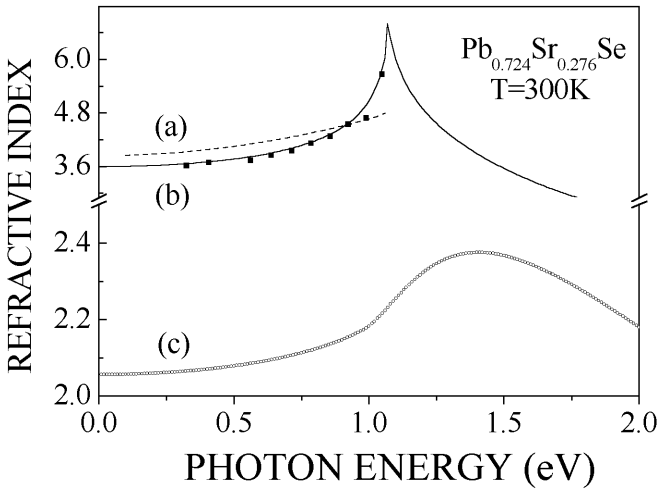

Figure 2. Comparison of some models with our experimental data (filled squares) at RT. (a) The dashed curve was obtained from a model using DiDomenico–Wemple parameters and a semi-empirical formula, (b) the solid curve was obtained using our Lorentz model, and (c) the dotted curve was obtained from the Tauc–Lorentz model.

where the amplitude constant A of 81.36 eV, the transition peak energy E_0 of 1.0211 eV, and the broadening term C [16] of 3.0 eV for $Pb_{0.724}Sr_{0.276}Se$ at RT are obtained from spectroscopic ellipsometry measurements, and the band gap E_g of 1.0644 eV is obtained from the FTIR absorption spectrum. Since A is the amplitude constant and C is the broadening constant, it is reasonable to take A and C to be constant for PbSrSe sample as temperature varies. As we know, the energy E_0 of the peak of the refractive index will change with the absorption band edge. We have changed the value of E_0 for the $Pb_{0.724}Sr_{0.276}Se$ sample at different temperatures in the fitting process. We find that the difference between E_g and E_0 remains almost constant, at 0.0433 eV, for $Pb_{0.724}Sr_{0.276}Se$ at any temperature. This is equal to the difference between E_g and E_0 from ellipsometry measurements for $Pb_{0.724}Sr_{0.276}Se$ at RT, so we have an empirical equation between E_g and E_0:

$$E_0 = E_g - 0.0433 \text{ (eV)}. \tag{3}$$

Equation (3) describes well the experimental results for our other samples (see figure 3 for different temperatures and figure 4(a) for samples with different Sr compositions), as well as the results in the literature [2] (see figure 4(b)).

The dielectric function $\varepsilon_1(E)$ is obtained by Kramers–Kronig integration:

$$\varepsilon_1(E) = \varepsilon_1(\infty) + \frac{2}{\pi} \mathrm{P} \int_{E_g}^{\infty} \frac{\xi \varepsilon_2(\xi)}{\xi^2 - E^2} \, \mathrm{d}\xi \tag{4}$$

where 'P' stands for the Cauchy principal part of the integral, and another fitting parameter, $\varepsilon_1(\infty)$, has been included. Furthermore, $\varepsilon_1(\infty)$ is found to vary with the absorption edge E_g, and can be expressed by means of the following empirical relationships:

$$\varepsilon_1(\infty) = 9.8 - 10.4(E_g/\text{eV}) \qquad E_g < 0.716 \text{ eV} \tag{5a}$$

and

$$\varepsilon_1(\infty) = 2.45 \qquad E_g \geqslant 0.716 \text{ eV} \tag{5b}$$

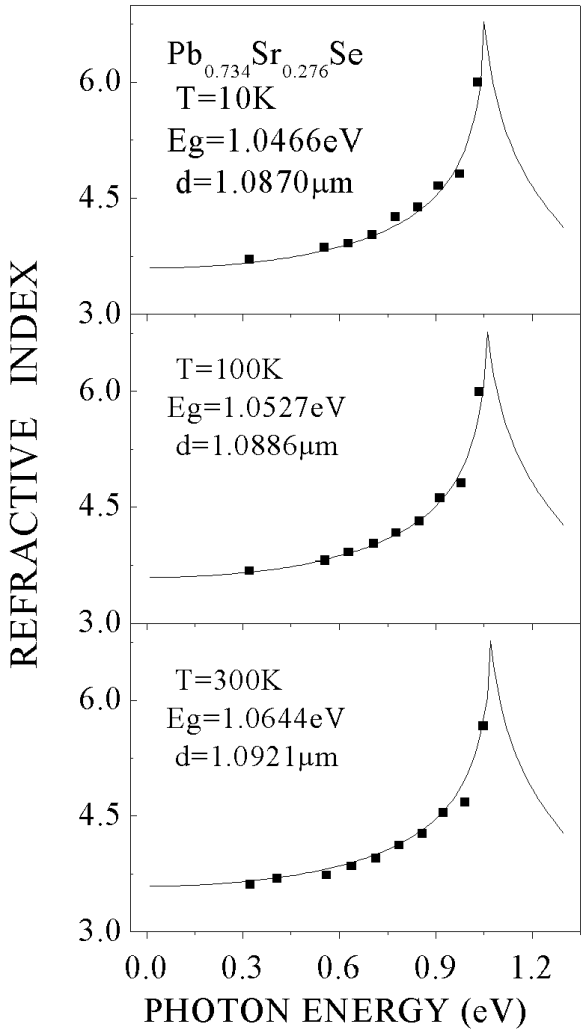

Figure 3. Temperature-dependent refractive indices in $Pb_{0.724}Sr_{0.276}Se$ thin film as a function of photon energy. Solid curves: theoretical results; solid squares: experimental data.

as shown in the inset of figure 4(b). Then the refractive index n and the extinction coefficient k are obtained as follows [17]:

$$n = \sqrt{\frac{\sqrt{\varepsilon_1^2 + \varepsilon_2^2} + \varepsilon_1}{2}} \tag{6a}$$

$$k = \sqrt{\frac{\sqrt{\varepsilon_1^2 + \varepsilon_2^2} - \varepsilon_1}{2}}. \tag{6b}$$

Therefore we can obtain the theoretical refractive index of PbSrSe with different compositions x at different temperatures from the model proposed above, with two fitting parameters, in relation to E_g, E_0 through equation (3)and $\varepsilon_1(\infty)$ through equation (5).

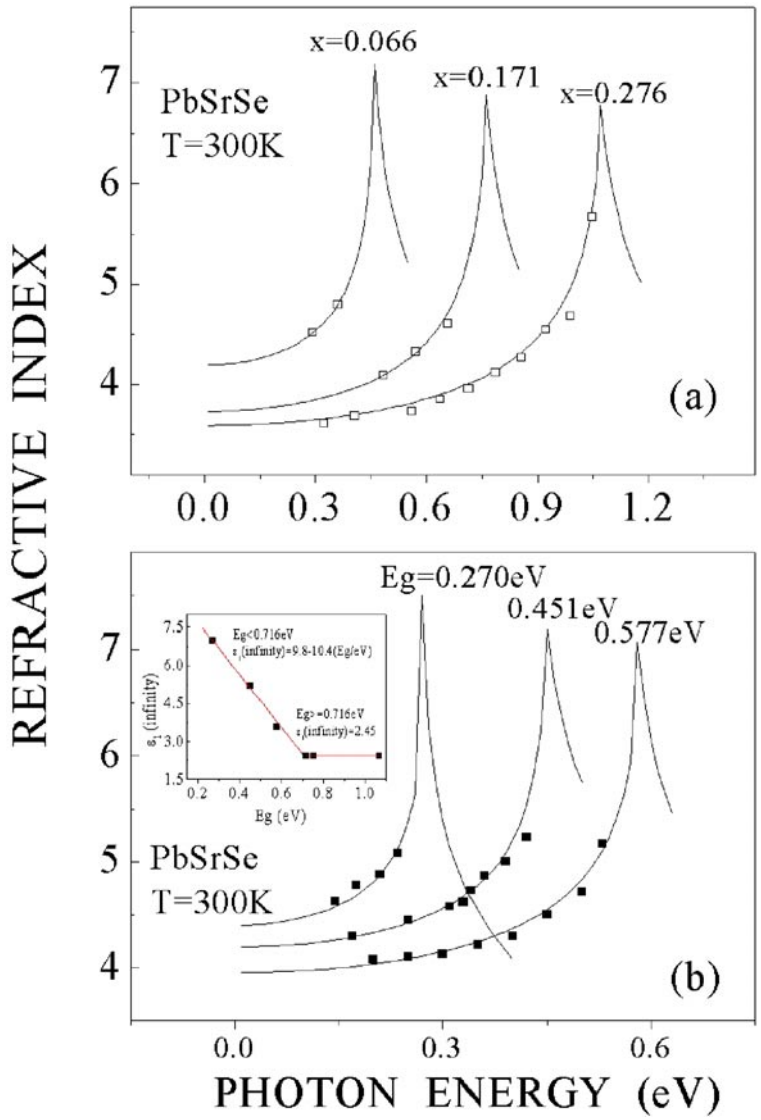

Figure 4. We show the calculated refractive index (solid curves) and our experimental data (open squares) with Sr contents 0.066 ($E_g = 0.441$ eV), 0.171 ($E_g = 0.752$ eV) and 0.276 ($E_g = 1.064$ eV) in (a); and the data from [2] (filled squares) in (b). Shown in the inset of (b) is the relation of $\varepsilon_1(\infty)$ with E_g that we obtained.

(This figure is in colour only in the electronic version)

4. Results and discussion

Figure 3 shows the refractive index of $Pb_{0.724}Sr_{0.276}Se$ at $T = 10$, 100, and 300 K versus photon energy. The filled squares show the experimental data, and the solid curves are the calculation results. In addition to the good agreement between the theory and experiment, we find that the refractive index below the absorption edge reduces with increase of the temperature. The $Pb_{0.724}Sr_{0.276}Se$ epitaxial layer thickness of 1.0921 μm at 300 K was obtained

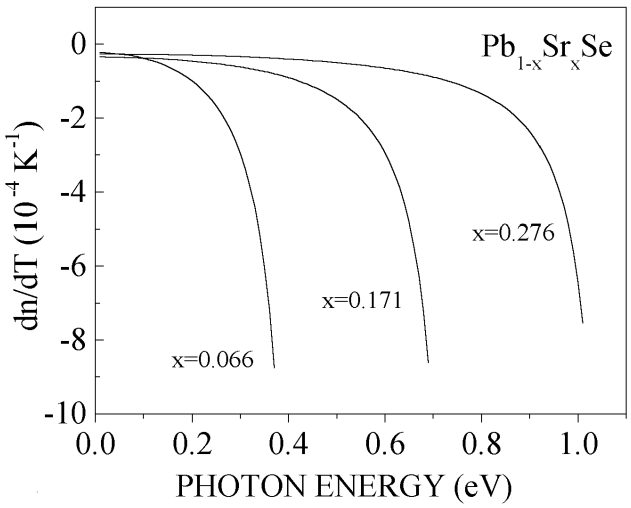

Figure 5. The calculated rate of change of the refractive index with temperature, $\mathrm{d}n/\mathrm{d}T$, as a function of photon energy below the band gap for the PbSrSe thin films.

from the spectroscopic ellipsometry measurements; the thicknesses of 1.0870 μm at 10 K and 1.0886 μm at 100 K were derived from the comparison of the experimental refractive index with the theoretical result (see figure 3). Figure 4 shows the dependence of the composition x (and band gap E_{g}) on the experimental refractive index at RT. The open squares in figure 4(a) represent our experimental results for $Pb_{1-x}Sr_xSe$ with $x = 0.066$, 0.171, and 0.276; the filled squares in figure 4(b) are from [2]. These are shown together with the solid curves representing our calculation results. It is obvious that our model can describe the refractive index—both our results and these reported in the literature—for $Pb_{1-x}Sr_xSe$ with x from 0 to 0.276 very well.

Figure 5 shows the dependence of $\mathrm{d}n/\mathrm{d}T$ on the photon energy and the composition x. It is clear that in the low-energy region, $\mathrm{d}n/\mathrm{d}T$ has a linear relationship with the photon energy, and its value is less than 1.0×10^{-4}. The value changes rapidly when the photon energy is close to the band-gap energy, as shown in figure 5, due to the rapid changes in the refractive index near E_{g}, where $\mathrm{d}n/\mathrm{d}T$ is close to the PbSe value of 8.2×10^{-4} K^{-1} [1].

From figures 3 and 4, we can see clearly that the refractive index n increases rapidly with the photon energy below the band-gap energy, while in the above-band-gap energy region, n decreases rapidly too. There is a maximum in the refractive index near E_{g}, which can be understood on the basis of the following equation [15]:

$$n(\nu) = 1 + \frac{c}{\pi}\int_0^{\infty} \frac{\mathrm{d}\alpha(\nu')}{\mathrm{d}\nu'} \log\left(\frac{\nu' + \nu}{\nu' - \nu}\right) \mathrm{d}\nu' \tag{7}$$

where c is the light velocity in vacuum, ν and ν' are photon frequencies, $\alpha(\nu)$ is the absorption coefficient. In the frequency region near the absorption edge the value of $\mathrm{d}\alpha(\nu')/\mathrm{d}\nu'$ is large; however, when the photon energy reaches the gap energy, the absorption curve changes its slope and becomes flatter, so the value of $\mathrm{d}\alpha(\nu')/\mathrm{d}\nu'$ decreases at the gap energy.

The rapid change in refractive index near the band gap provides a large refractive index step between the active and cladding regions, useful for laser design. Furthermore, we know that the sample with the smaller Sr composition has the larger refractive index. Figure 6(a) shows the calculation results (solid curve) as a function of Sr composition at RT, together with the experimental results near $E_{\mathrm{g}}/2$ (filled circles). Similar results have been observed

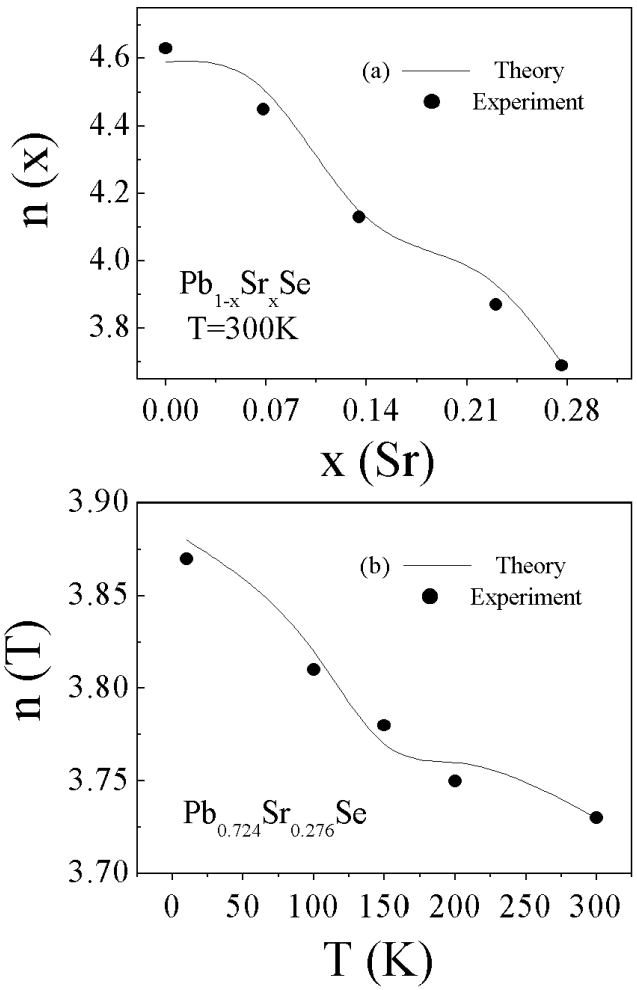

Figure 6. (a) The composition-dependent refractive index near $E_g/2$ at 300 K (filled circles for experimental data, the solid curve for calculated results). (b) The temperature-dependent refractive index near $E_g/2$ for $Pb_{0.724}Sr_{0.276}Se$ (filled circles for experimental data, the solid curve for calculated results).

for $In_{1-x}Ga_xAs_yP_{1-y}$ [18]. We can also observe that the refractive index decreases with the increase of temperature, as demonstrated in figure 6(b) where the good agreement between the theoretical calculation (solid curve) and experimental results for the $Pb_{0.724}Sr_{0.276}Se$ sample near $E_g/2$ (filled circles) is clearly revealed.

Figure 7 shows the extinction coefficient k as a function of photon energy. It is clear that the peak energy of the extinction coefficient (E_{kp}) for $Pb_{1-x}Sr_xSe$ increases with the Sr composition ((a) for $x = 0.276$, (b) for $x = 0.171$, (c) for $x = 0.135$, (d) for $x = 0.066$) and the sample with a larger Sr composition has a larger maximum extinction coefficient. On the basis of the calculation results, the difference between the peak energy E_{kp} and the band-gap energy E_g can be expressed, as shown in the inset of figure 7, as

$$(E_{kp} - E_g)/\text{eV} = -0.115 + \frac{0.159}{[(E_g/\text{eV}) - 1.0376]^2 + 1.2954}. \tag{8}$$

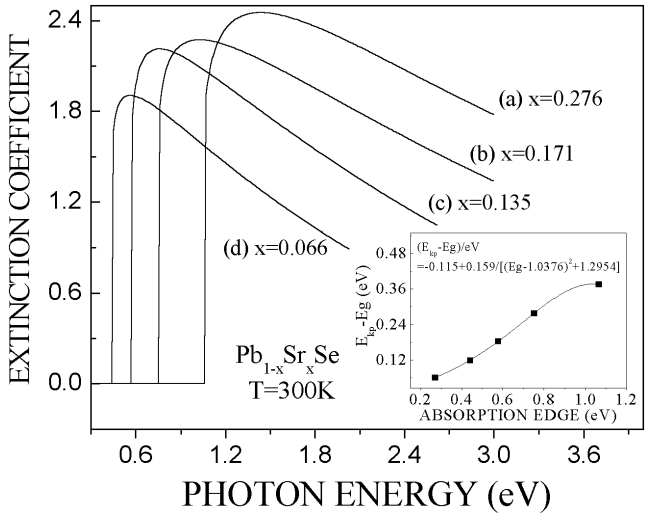

Figure 7. The composition-dependent extinction coefficient for $Pb_{1-x}Sr_xSe$ thin films at RT: (a) $x = 0.276$, (b) $x = 0.171$, (c) $x = 0.135$, (d) $x = 0.066$. Shown in the inset is the difference between the peak energy E_{kp} of the extinction coefficient and E_g in relation to the band gap E_g.

Finally, we discuss the thermal expansion coefficient α_{PbSrSe} of PbSrSe. Figure 8 shows the dependence of the thickness of PbSrSe thin films on temperature. From [3] we have the thermal expansion coefficient α_{PbSe} of PbSe: $19.4 \times 10^{-6}\ K^{-1}$. The thermal expansion coefficient α_{SrSe} of SrSe is also an important parameter, but is still not available in the literature [3]. According to [7], the ternary system's physical parameter Q can be given as

$$Q_{A_{1-x}B_xC} = xQ_{BC} + (1-x)Q_{AC} \tag{9}$$

where x is the composition. From equation (12) we can get α_{PbSrSe}:

$$\alpha_{Pb_{1-x}Sr_xSe} = x\alpha_{SrSe} + (1-x)\alpha_{PbSe} \tag{10}$$

and the relation between the film thickness and the thermal expansion coefficient of PbSrSe can be expressed as

$$d(T) = d_{300\ K}[1 - \alpha_{Pb_{1-x}Sr_xSe}(300 - T)] \tag{11}$$

where $d_{300\ K}$ is the film thickness at 300 K, $d(T)$ is the film thickness at temperature T. Since we have obtained the thickness of $Pb_{1-x}Sr_xSe$ epitaxial layers at different temperatures, as shown in figure 8, we can get $\alpha_{SrSe} = 7.3 \times 10^{-6}\ K^{-1}$ for a $Pb_{0.724}Sr_{0.276}Se$ thin-film sample via comparing equation (11) with the linear fitting equation for thickness shown in figure 8, and by the same method we obtain $\alpha_{SrSe} = 7.1 \times 10^{-6}\ K^{-1}$ for $Pb_{0.829}Sr_{0.171}Se$ thin film and $7.6 \times 10^{-6}\ K^{-1}$ for $Pb_{0.934}Sr_{0.066}Se$ thin film. The good agreement for α_{SrSe} among the three samples strongly supports the reliability of the thermal expansion coefficient obtained for SrSe: $(7.3 \pm 0.3) \times 10^{-6}\ K^{-1}$, as well as the experimental results and the model described in this paper.

5. Conclusions

In summary, the optical constants of $Pb_{1-x}Sr_xSe$ thin films were studied by means of temperature-dependent FTIR absorption measurements. The experimental refractive indices were deduced via Fabry–Pérot interference fringes in FTIR absorption spectra. A new and

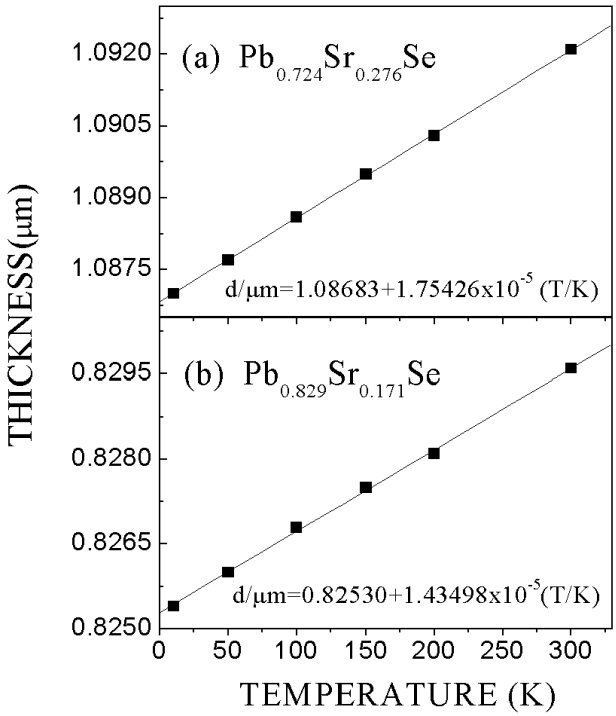

Figure 8. The thicknesses of $Pb_{0.724}Sr_{0.276}Se$ (a) and $Pb_{0.829}Sr_{0.171}Se$ (b) thin films as functions of temperature.

simple model was presented for obtaining the theoretical refractive index and extinction coefficient in relation to the band-gap energy. The model is in good agreement with our experimental results for $Pb_{1-x}Sr_xSe$ ($0.066 \leqslant x \leqslant 0.276$, 10 K $\leqslant T \leqslant$ 300 K) thin films, as well as the reported results for $Pb_{1-x}Sr_xSe$ ($0 \leqslant x \leqslant 0.23$, $T = 300$ K) thin films. The SrSe thermal expansion coefficient of $(7.3 \pm 0.3) \times 10^{-6}$ K^{-1} was obtained here for the first time, with the aid of a temperature-dependent film thickness and a linear interpolation scheme. We think that the results obtained here will be very useful in the design of PbSe- and/or PbSrSe-based laser structures.

Acknowledgments

This work was supported in part by the Natural Science Foundation of China under the contracts 10125416, 60006005, TRAPOYT and Shanghai QMX project 00QA14012. The authors would like to acknowledge Dr H Z Wu at the University of Oklahoma for providing the samples and Mr L G Zhu at Shanghai Jiao Tong University for technical help.

References

[1] McCann P J, Namjou K and Fang X M 1999 *Appl. Phys. Lett.* **75** 3608
[2] Fang X M, Namjou K, Chao I N, McCann P J and Tor G 2000 *J. Vac. Sci. Technol.* B **18** 1720
[3] Xu G, Fang X M, McCann P J and Shi Z 2000 *J. Cryst. Growth* **209** 763
[4] Lambrecht A, Herres N, Spanger B, Kuhn K, Böttner H, Tacke M and Evers J 1991 *J. Cryst. Growth* **108** 301
[5] McCann P J, Li L, Fumeaux J E and Wright R 1995 *Appl. Phys. Lett.* **66** 1355

[6] Fuchs F and Koidl P 1991 *Semicond. Sci. Technol.* **6** C71
[7] Casey H C Jr and Panish M B 1978 *Heterostructure Lasers* (New York: Academic) Parts A and B
[8] Herrmann K H 1997 *SPIE* **3182** 195
[9] Herrmann K H, Muller U and Melzer V 1993 *Semicond. Sci. Technol.* **8** S330
[10] Sachar H K, Chao I N, McCann P J and Fang X M 1999 *J. Appl. Phys.* **85** 7398
[11] Shen W Z, Yang H F, Jiang L F, Wang K, Yu G, Wu H Z and McCann P J 2002 *J. Appl. Phys.* **91** 192
[12] Pankove J I 1975 *Optical Processes in Semiconductors* (New York: Dover)
[13] Tomm J W, Möllmann K-P, Peuker F, Herrmann K H, Böttner H and Tacke M 1994 *Semicond. Sci. Technol.* **9** 1033
[14] Afromowitz M A 1974 *Solid State Commun.* **15** 59
[15] Liu K, Chu J H and Tang D Y 1994 *J. Appl. Phys.* **75** 4176
[16] Jellison G E Jr and Modine F A 1996 *Appl. Phys. Lett.* **69** 371
[17] Huang Z M and Chu J H 2001 *Infrared Phys. Technol.* **42** 77
[18] Adachi S 1982 *J. Appl. Phys.* **53** 5863